Analytical Design of Microstrip Short-Circuit Terminated Stepped-Impedance Resonator Dual-Band Filters

Wei-Shin Chang and Chi-Yang Chang, *Member, IEEE*

***Abstract*—This paper proposes an analytical method to design a dual-band filter using the short-circuit terminated half-wavelength stepped-impedance resonator (SIR). The SIR has an advantage to easily control the first and second resonances by adjusting its structural parameters. In the proposed method, the structural parameters of the SIR are obtained analytically according to the two passband center frequencies and bandwidths of the filter. As a result, the achievable specifications of the dual-band filter can be rapidly determined. The coupling between adjacent SIRs is realized by a short-circuited stub, which is characterized as a K-inverter network. The dual-frequency transformer incorporated with the tapped-line input/output structure is used for the external coupling. Applying the analytical equations in the design process, a dual-band filter can be easily and quickly realized. More importantly, compared to the published dual-band filters, the proposed method is easier to design, especially for a relatively high-order dual-band filter. Two fourth-order and one sixth-order dual-band filters are designed and fabricated to demonstrate the proposed method.**

***Index Terms*—Bandpass filter (BPF), dual band, microstrip, stepped-impedance resonator (SIR).**

I. Introduction

BANDPASS filters (BPFs) are essential components in wireless communication systems. The planar filter has an important role in the RF circuit design due to the low fabrication cost and easy integration into the printed circuit board (PCB). Recently, due to the increasing demand for dual-band operation in modern RF systems, dual-band filters have become an essential component. The most straightforward method to implement a dual-band filter is to combine two BPFs with individual passbands using additional impedance-matching networks [1]. However, this circuit usually has the area larger than twice that of the single-band filter and may suffer from the extra loss. Therefore, to save the circuit area and cost, it is more appropriate to design an integrated filter capable of operating in two passbands.

Manuscript received October 18, 2010; revised March 03, 2011; accepted March 04, 2011. Date of publication April 25, 2011; date of current version July 13, 2011. This work was supported in part by the National Science Council, Taiwan, under Grant NSC 98-2221-E-009-034-MY3 and Grant NSC 99-2221-E-009-050-MY3.

The authors are with the Graduate Institute of Communication Engineering, National Chiao-Tung University, Hsinchu 300, Taiwan (e-mail: aa494412338@hotmail.com; mhchang@cc.nctu.edu.tw).

Color versions of one or more of the figures in this paper are available online at http://ieeexplore.ieee.org.

Digital Object Identifier 10.1109/TMTT.2011.2132140

There are many methods to design dual-band filters. The cascade connection of a bandpass and a bandstop filter is used to achieve a dual-band performance [2]. The dual-band filter can also be realized using the resonators consisting of the open- or short-circuited stubs, which are placed in series or in parallel to create transmission zeros in the middle passband of a wideband BPF [3]–[5]. These circuits have high skirt selectivity, but they usually require a complex design procedure and have a large circuit area due to the many series or shunt stubs. On the other hand, the two passbands in [2] could not be far apart from each other, which may be inconvenient in practical applications. In [3]–[5], the stopband rejection is limited since shunt stubs only have narrow bandstop characteristics. Moreover, there are undesired passbands below the first passband and above the second passband. Although the stopband performance can be improved by using series stubs [4], series transmission line components are difficult to realize so that they have to be replaced by coupled-line sections. Another method to design dual-band filters is to combine two individual resonators using the common input and output ports [6]–[9]. These circuits may occupy a large area or have complex structures. Furthermore, the passband frequencies and bandwidths are usually limited since the order of the filter may be difficult to increase. Stub-loaded resonators are also adopted in the dual-band filter design since they are simple in structure [10]–[12]. However, it is difficult to adjust the coupling coefficient between resonators to simultaneously meet the dual bandwidth specifications of the filter.

Stepped-impedance resonators (SIRs) have been widely used to realize dual-band filters [13]–[21]. The SIR is very attractive due to its controllable resonant frequencies, simple structure, and well-established design method. Theoretical analysis reveals that the fundamental and second resonances of the SIR are easily controlled by adjusting the structural parameters [22]. However, the first step of the conventional method to design a SIR dual-band filter is to draw the design graphs of coupling coefficients for each pair of SIRs. Consequently, the feasible bandwidths of the dual-band filter are determined by the overlap region of the design graphs. To find each point on the design graph, a full-wave electromagnetic (EM) simulation software must be used to calculate the coupling coefficient since the coupling between adjacent SIRs is via coupled-line sections. In addition, for the same first and second resonances, there are many choices of SIR parameters. Different design graphs are necessary for different structural parameters of SIRs. As a result, it is very time consuming to construct design graphs. Furthermore, as the order of the filter is larger than three, more than one design graph

is required. This method might be inefficient to design a relatively high-order dual-band filter (i.e., more than fourth order). On the other hand, in the filter design process, knowing the feasible bandwidth first for specific pairs of SIRs contradicts the regular design procedure. Generally speaking, the implementation process is to know the filter specifications first and then obtain the filter structure. Although there are many studies related to SIR dual-band filters, there still lacks an efficient and time-saving design procedure.

In this paper, we present a simple and time-saving method to design a SIR dual-band filter. Here, a short-circuit terminated half-wavelength SIR is used. First, the structural parameters of the SIR can be determined according to the two center frequencies and bandwidths of the dual-band filter. The coupling between adjacent SIRs is then realized by a short-circuited stub, which works as a K-inverter. Thus, the closed-form equations for the coupling strength are derived. The method shown here is very different from those in [13]–[21], where the coupling coefficient and the available bandwidth are limited by the preselected SIR structure. In addition, by using the short-circuited stub, the achievable coupling strength between SIRs is much less constrained compared to that by using coupled-line sections since the gap between coupled lines is seriously limited. The proposed method follows the regular design procedure, namely, determining the filter specifications first and then choosing appropriate resonator structures. Accordingly, the feasible specifications of the dual-band filter are able to be rapidly checked in advance. On the basis of this analytical method, a dual-band filter can be quickly realized and is easily simulated using the conventional circuit simulator, especially for a relatively high-order dual-band filter. Finally, we design two fourth-order and one sixth-order dual-band filters to illustrate the proposed method.

II. Characteristics of the Short-Circuit Terminated Half-Wavelength SIR

The SIR has the ability to control the first and second resonant frequencies [22]. Fig. 1 shows the short-circuit terminated half-wavelength SIR, where Z_1 and Z_2 are the characteristic impedances of the microstrip sections and θ_1 and θ_2 are the respective electrical lengths. The input impedance seen from the middle of the SIR is

$$Z_{\text{in}} = jZ_1 \frac{Z_2 \tan\theta_2 + Z_1 \tan\theta_1}{Z_1 - Z_2 \tan\theta_1 \tan\theta_2}. \tag{1}$$

Therefore, the fundamental frequency f_1 and the first spurious frequency f_2 of the SIR are determined by the first roots of the following equations:

$$R\tan\theta_1 \tan\theta_2 - 1 = 0, \qquad \text{for } f_1 \tag{2}$$

$$R\tan\theta_2 + \tan\theta_1 = 0, \qquad \text{for } f_2 \tag{3}$$

where $R = Z_2/Z_1$ is the impedance ratio of the SIR. If $f_2 \geq 2f_1$ is required, $R \geq 1$ should be chosen and vice versa. Thus, the passband center frequencies of the dual-band filter (i.e., f_1 and f_2) can be controlled by the impedance ratio R and the electrical length ratio of θ_1 and θ_2.

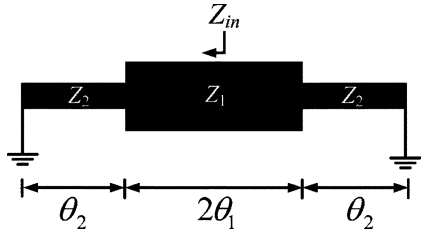

Fig. 1. Structure of the short-circuit terminated half-wavelength SIR.

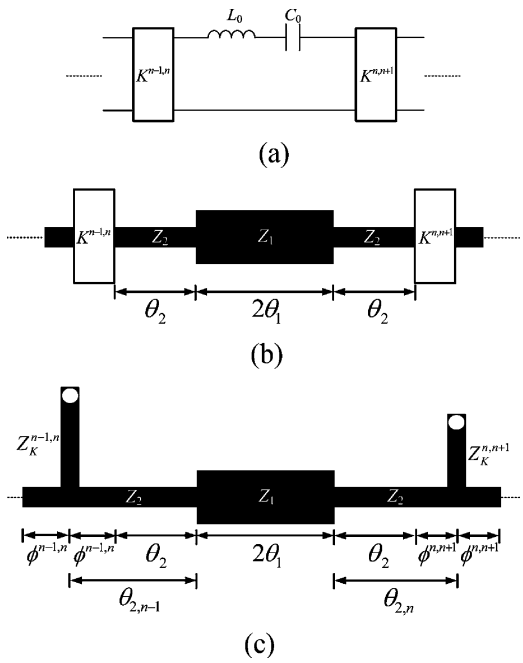

Fig. 2. Configuration of the nth resonator in the proposed filter. (a) BPF circuit with series resonators and impedance inverters. (b) Dual-band filter using short-circuit terminated half-wavelength SIRs and K-inverters. (c) Microstrip implementation of the dual-band filter.

III. Design Process and Configuration of the Dual-Band Filter

In this study, there are N resonators in the Nth-order filter. Fig. 2(a) shows a generalized BPF circuit using impedance inverters [23]. The series resonant circuit can be replaced by a short-circuit terminated half-wavelength SIR. The configuration of the nth resonator in the proposed filter is shown in Fig. 2(b) and (c), where n is from 1 to N. The coupling between the nth and $(n+1)$th resonators is represented by the K-inverter (i.e., $K^{n,n+1}$). Since all resonators in the filter have the same structure, their reactance slope parameters x [23] are equal at the specific frequency. In the design process, first, the filter specifications (i.e., center frequencies and bandwidths) are given. Choose a proper set of SIR structural parameters that correspond to two passband center frequencies and appropriate reactance slope parameters. The value of the K-inverter between SIRs is then calculated according to each passband bandwidth. The K-inverter is implemented by a short-circuited stub and its parameters can

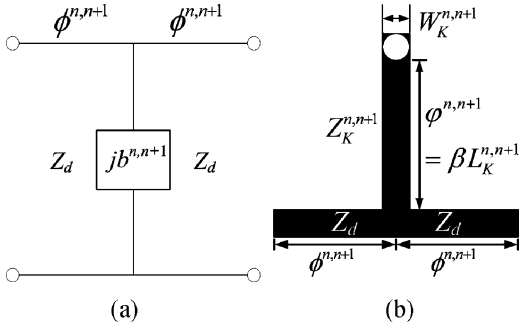

Fig. 3. (a) Equivalent circuit model of the K-inverter. (b) Microstrip realization of the K-inverter.

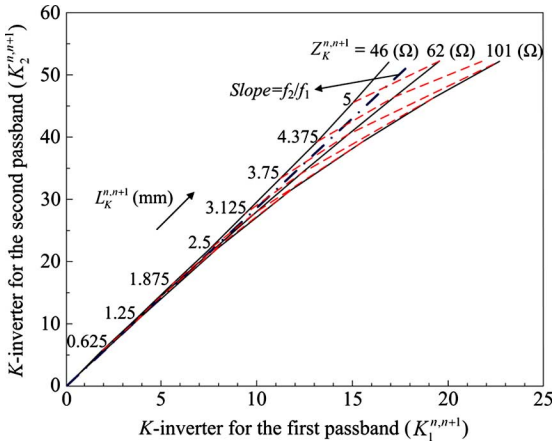

Fig. 4. K values of the first and second passbands versus $Z_K^{n,n+1}$ and $L_K^{n,n+1}$ for $f_1 = 1.8$ GHz, $f_2 = 5.2$ GHz, and $Z_d = 86\ \Omega$.

be obtained by the design equations. Finally, by combining the SIRs and K-inverters along with the proper input and output ports, the dual-band filter is completed. The detailed discussion is in the following paragraphs. Here, g_0, g_n, and g_{n+1} are the element values of the low-pass filter prototype.

A. K-Inverter

Since the short-circuit terminated half-wavelength SIR is adopted in the filter, the short-circuited stub can be straightforwardly used as the K-inverter between resonators. Each K-inverter value corresponding to the filter specifications is obtained as [23]

$$K^{n,n+1} = \Delta\sqrt{\frac{x^2}{g_n g_{n+1}}}. \tag{4}$$

Fig. 3(a) shows an equivalent K-inverter circuit where a shunt susceptance $b^{n,n+1}$ is included. The shunt susceptance can be implemented by a microstrip short-circuited stub, as shown in Fig. 3(b). In Fig. 3(b), Z_d and $Z_K^{n,n+1}$ are the characteristic impedances of the input/output transmission line and the short-circuited stub, respectively, while $\phi^{n,n+1}$ and $\varphi^{n,n+1}$ are the respective electrical lengths. By comparing the $ABCD$ matrix, the relations between the K-inverter and its equivalent circuit are obtained as [23]

$$K^{n,n+1} = Z_d \tan\left|\phi^{n,n+1}\right| \tag{5}$$

$$b^{n,n+1} = \frac{\left(K^{n,n+1}/Z_d\right)^2 - 1}{K^{n,n+1}} \tag{6}$$

$$\phi^{n,n+1} = -\frac{1}{2}\tan^{-1}\left|\frac{2}{b^{n,n+1}Z_d}\right|. \tag{7}$$

Neglecting the T-junction effect in Fig. 3(b), the shunt susceptance can be derived as

$$\begin{aligned} jb^{n,n+1} &= -j\frac{1}{Z_K^{n,n+1}}\cot(\varphi^{n,n+1}) \\ &= -j\frac{1}{Z_K^{n,n+1}}\cot(\beta L_K^{n,n+1}) \end{aligned} \tag{8}$$

where $\beta = \omega\sqrt{\mu\epsilon}$ is the propagation constant. In Fig. 3(b), the higher the impedance Z_d is (i.e., narrower linewidth), the smaller the T-junction effect is. For simplicity, we ignore the influence of the T-junction effect on the K-inverter in the following discussion.

In this paper, we choose $Z_d = Z_2$ since the K-inverter is connected to the end of the SIR. For the dual-band filter, since β is dependent on the operating frequency, from (6) and (8), the K-inverter in Fig. 3 leads to different K values in two passbands (i.e., $K_1^{n,n+1}$ for the first passband and $K_2^{n,n+1}$ for the second passband). Moreover, the longer the length $L_K^{n,n+1}$ is, the larger the values $K_1^{n,n+1}$ and $K_2^{n,n+1}$ are. It should be noted that in the practical application, $L_K^{n,n+1} \ll \lambda$, the ratio of K values is approximately equal to the ratio of center frequencies. This is because when $L_K^{n,n+1} \ll \lambda$, $\cot(\beta L_K^{n,n+1}) \approx 1/(\beta L_K^{n,n+1})$. The K value is also very small under this condition so that $(K^{n,n+1}/Z_d)^2 \ll 1$. Consequently, from (6) and (8), $\beta L_K^{n,n+1} \approx K^{n,n+1}/Z_K^{n,n+1}$. The following relationship is approximately held:

$$\frac{f_2}{f_1} = \frac{\beta_2}{\beta_1} = \frac{\varphi^{n,n+1}|_{f=f_2}}{\varphi^{n,n+1}|_{f=f_1}} \approx \frac{K_2^{n,n+1}}{K_1^{n,n+1}} \tag{9}$$

where β_1 is the propagation constant for the first passband and β_2 is that for the second passband. This relationship is very useful to simplify the filter design.

To demonstrate (9), according to (6) and (8), Fig. 4 plots $K_1^{n,n+1}$ and $K_2^{n,n+1}$ versus $Z_K^{n,n+1}$ and $L_K^{n,n+1}$ under the condition $f_1 = 1.8$ GHz, $f_2 = 5.2$ GHz, and $Z_d = 86\ \Omega$ for the substrate with a dielectric constant of 3.6 and a thickness of 0.508 mm. The dashed–dotted line corresponds to $K_2^{n,n+1}/K_1^{n,n+1} = f_2/f_1$. It is observed in Fig. 4 that as $K_1^{n,n+1}$ is smaller than 8.5 for any value of $Z_K^{n,n+1}$, (9) is valid. Take $\theta_1 = 0.5001$ rad, $\theta_2 = 0.6495$ rad, and $Z_1 = 35.68\ \Omega$ as an example. These values are chosen based on the two passband center frequencies and bandwidths of the filter to make (9) valid, which will be discussed later. If a dual-band filter with a fourth-order Chebyshev frequency response and a 0.1-dB ripple level is designed, $K_1^{1,2} = 8.5$ and $K_2^{1,2} = 24.56$ correspond to the fractional bandwidths of approximately 10% for the first passband and 7% for the second passband, respectively. This can fulfill most of the communication applications. When the K value becomes larger, one can use Fig. 4 to find a point on the

dashed–dotted line that matches the large K value and satisfies $K_2^{n,n+1}/K_1^{n,n+1} = f_2/f_1$. In other words, a specific $Z_K^{n,n+1}$ can always be chosen to make $K_2^{n,n+1}/K_1^{n,n+1} = f_2/f_1$. It should be emphasized that for the large K value (i.e., in the broadband situation), the equivalent K-inverter circuit itself becomes inadequate and the final fine tuning for the filter is required.

Now, taking the inverter $K^{n,n+1}$ in Fig. 2 as an example, the electrical length $\theta_{2,n}$ should be equal to $\theta_2 + \phi^{n,n+1}$, where $\phi^{n,n+1}$ has a negative sign. To keep the physical structures fixed at two frequencies, the following relationship should be held:

$$\frac{\theta_{2,n}|_{f=f_2}}{\theta_{2,n}|_{f=f_1}} = \frac{(\theta_2 + \phi^{n,n+1})|_{f=f_2}}{(\theta_2 + \phi^{n,n+1})|_{f=f_1}} = \frac{f_2}{f_1}. \tag{10}$$

In the following discussion, we denote $\phi^{n,n+1}|_{f=f_1}$ as $\phi_1^{n,n+1}$ and $\phi^{n,n+1}|_{f=f_2}$ as $\phi_2^{n,n+1}$ for simplicity. According to (10), the electrical length of the input/output transmission line in Fig. 3 should have the relation of $\phi_2^{n,n+1}/\phi_1^{n,n+1} = f_2/f_1$. In practice, there are two situations to consider, which are: 1) $\phi_2^{n,n+1}/\phi_1^{n,n+1} \approx f_2/f_1$ and 2) $\phi_2^{n,n+1}/\phi_1^{n,n+1} \neq f_2/f_1$.

1) $\phi_2^{n,n+1}/\phi_1^{n,n+1} \approx f_2/f_1$: This condition occurs when the K value is small or $L_K^{n,n+1} \ll \lambda$. In the narrowband application, $L_K^{n,n+1}$ is much smaller than λ so that $\beta L_K^{n,n+1}$ is very small. Equations (7) and (8) become

$$\phi^{n,n+1} \approx -\frac{Z_K^{n,n+1}\beta L_K^{n,n+1}}{Z_d}. \tag{11}$$

Since $Z_K^{n,n+1}$, Z_d, and $L_K^{n,n+1}$ are all fixed, $\phi_2^{n,n+1}/\phi_1^{n,n+1} \approx \beta_2/\beta_1 = f_2/f_1$. The physical lengths of $\phi_1^{n,n+1}$ and $\phi_2^{n,n+1}$ are the same.

2) $\phi_2^{n,n+1}/\phi_1^{n,n+1} \neq f_2/f_1$: As the fractional bandwidth becomes larger, the linear relationship between $\phi^{n,n+1}$ and f cannot hold any more. In most of the larger fractional bandwidth situations, $|\phi_1^{n,n+1}| < f_1|\phi_2^{n,n+1}|/f_2$ is true.

When $|\phi_1^{n,n+1}| < f_1|\phi_2^{n,n+1}|/f_2$, the corresponding reduced physical lengths of θ_2 at two passbands are different. Let the physical length of $\theta_{2,n}$ corresponding to $\phi_2^{n,n+1}$ be first determined (i.e., $\theta_{2,n}|_{f=f_2} = \theta_2|_{f=f_2} + \phi_2^{n,n+1}$). An open stub is then added in the middle of the SIR where the electrical characteristics at f_2 are unaffected, as shown in Fig. 5(a). In Fig. 5(a), the open stub has the characteristic impedance Z_3 and the electrical length θ_3. To reduce the influence of the open stub on the SIR at f_2, its width should be as small as possible (i.e., large Z_3). It will be shown later that the insufficient electrical length of the SIR at f_1 is compensated by the open stub.

In Fig. 5(b), the resonant condition of the equivalent SIR at f_1 is $Y_{\text{in}} = 0$. Since the physical length of $\theta_{2,n}$ is based on $\phi_2^{n,n+1}$, it becomes too short for the first passband. Moreover, the electrical length θ_{2S} in Fig. 5(c) can be obtained as

$$\theta_{2S} = \theta_{2,n}|_{f=f_1} - \phi_1^{n,n+1} < \theta_2|_{f=f_1}. \tag{12}$$

However, in Fig. 5(c), the resonant condition of the open stub loaded SIR at f_1 is

$$Y'_{\text{in}} = Y_1\frac{-jY_2\cot\theta_{2S} + jY_1\tan\theta_1}{Y_1 + Y_2\tan\theta_1\cot\theta_{2S}} + j\frac{Y_3}{2}\tan\theta_3 = 0. \tag{13}$$

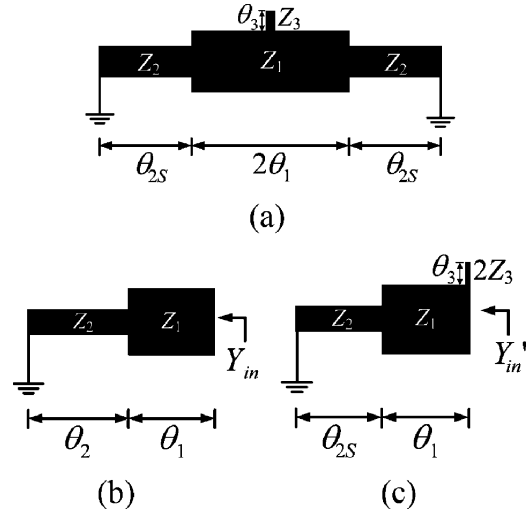

Fig. 5. Compensation for the electrical length of the first passband. (a) Structure of the stub-loaded SIR. (b) First resonance of the SIR without an open stub. (c) First resonance of the SIR with an open stub.

Hence, the open stub compensates for the insufficient length of the SIR at f_1, but has a negligible effect on the SIR at f_2. The electrical length θ_3 can be determined from (13) for the prescribed Z_3. In practical design, because the compensation is usually small, the open stub is very short. As a result, the open stub can be added to fine tune the whole filter performance in the final circuit simulation step.

B. Determination of the Structural Parameters of the SIR

In (2) and (3), there are numerous solutions (i.e., different R and electrical length ratio) for the specific frequencies f_1 and f_2. Now, we discuss how to choose the appropriate structural parameters of the SIR according to the prescribed filter specifications. In this paper, to simplify the design process, the element values of the low-pass filter prototype for two passbands are chosen to be identical (i.e., the same ripple level for two passbands). Thereby, from (4), the ratio of the fractional bandwidths is calculated as

$$\frac{\Delta_2}{\Delta_1} = \frac{K_2^{n,n+1}/\sqrt{(x_2)^2/g_n g_{n+1}}}{K_1^{n,n+1}/\sqrt{(x_1)^2/g_n g_{n+1}}} = \frac{K_2^{n,n+1}x_1}{K_1^{n,n+1}x_2} \tag{14}$$

where Δ_1 is the fractional bandwidth for the first passband and Δ_2 is that for the second passband. x_1 and x_2 are the reactance slope parameters seen from one end of the SIR at f_1 and f_2, respectively.

As mentioned in Section III-A, $K_2^{n,n+1}/K_1^{n,n+1} = f_2/f_1$ is always valid so as to simplify the design process. Therefore, (14) is further reduced to

$$x_1/x_2 = \frac{\Delta_2/\Delta_1}{f_2/f_1}. \tag{15}$$

Equation (15) indicates that once the filter specifications (i.e., f_1, f_2, Δ_1, and Δ_2) are given, x_1/x_2 is obtained. The input

impedance $Z_{\rm in}^{\rm SIR}$ and the reactance slope parameter x of the SIR shown in Fig. 6 are calculated as follows:

$$Z_{\rm in}^{\rm SIR} = jX = jZ_2\frac{A}{B} \tag{16}$$

$$x = \frac{\omega}{2}\frac{\partial X}{\partial \omega}|_{\omega=\omega_0} = \frac{Z_2}{2}\frac{C}{B^2} \tag{17}$$

$$A = 2R\tan\theta_2 + \tan 2\theta_1 - R^2\tan 2\theta_1 \tan^2\theta_2 \tag{18}$$

$$B = R - R^2\tan 2\theta_1\tan\theta_2 - R\tan^2\theta_2 - \tan 2\theta_1\tan\theta_2 \tag{19}$$

$$\begin{aligned} C = {} & (1+\tan^2\theta_2)(2R\theta_1\sec^2 2\theta_1 + 2R^2\theta_2\sec^2\theta_2 \\ & + 2R^3\theta_1\sec^2 2\theta_1\tan^2\theta_2 + R^2\theta_2\tan^2 2\theta_1\sec^2\theta_2) \\ & + \theta_2\tan 2\theta_1\sec^2\theta_2(\tan 2\theta_1 + 2R\tan\theta_2 - 2R^3\tan\theta_2 \\ & + R^4\tan 2\theta_1\tan^2\theta_2). \end{aligned} \tag{20}$$

For the SIR, the electrical length ratio α is defined as

$$\alpha = \frac{\theta_2}{\theta_1+\theta_2}. \tag{21}$$

The ratio of the reactance slope parameters is

$$\frac{x_1}{x_2} = \frac{\frac{Z_2}{2}\frac{C_1}{B_1^2}}{\frac{Z_2}{2}\frac{C_2}{B_2^2}} = \frac{C_1/B_1^2}{C_2/B_2^2} = f(\alpha, R) \tag{22}$$

where B_1 and C_1 are the values of (19) and (20), respectively, for f_1, while B_2 and C_2 are those for f_2. On the basis of α, R, (2) and (3), we can obtain $\theta_{1,f1}$, $\theta_{2,f1}$, $\theta_{1,f2}$, and $\theta_{2,f2}$, where $\theta_{1,f1}$ and $\theta_{2,f1}$ are the electrical lengths θ_1 and θ_2, respectively, for the first passband and $\theta_{1,f2}$ and $\theta_{2,f2}$ are those for the second passband. Thus, the ratio of x_1 and x_2 is a function of α and R. The ratio of the center frequencies is

$$\frac{f_2}{f_1} = \frac{\theta_{1,f2}}{\theta_{1,f1}} = g(\alpha, R). \tag{23}$$

Accordingly, the ratio of f_1 and f_2 can be expressed in terms of α and R.

From (19)–(23), Fig. 6 shows f_2/f_1 versus x_1/x_2 for different structural parameters of SIRs. Hence, the structure of the SIR can be determined from Fig. 6 as long as the filter specifications are given. On the other hand, for a fixed f_2/f_1 ratio, different combinations of R and α lead to different x_1/x_2, which corresponds to different Δ_2/Δ_1. With the aid of Fig. 6, the structure of the SIR can be quickly obtained and the available filter specifications are able to be predetermined. Consider the following dual-band filter specifications: $f_1 = 1.8$ GHz, $f_2 = 5.2$ GHz, $\Delta_1 = 0.13$, and $\Delta_2 = 0.09$. With these specifications, we calculate $f_2/f_1 = 2.89$ and $\Delta_2/\Delta_1 = 0.69$. From (15), we then obtain $x_1/x_2 = 0.24$. Therefore, according to Fig. 6, $R = 2.41$ and $\alpha = 0.565$ should be chosen. Apparently, the constraint of the curves in Fig. 6 is that as f_2/f_1 is close to 2, the choice of the SIR parameters becomes small. The extreme case is that when a uniform-impedance resonator (UIR) is chosen at $f_2/f_1 = 2$, the curves in Fig. 6 shrink to a point. This means that Δ_2/Δ_1 must be equal to 1.

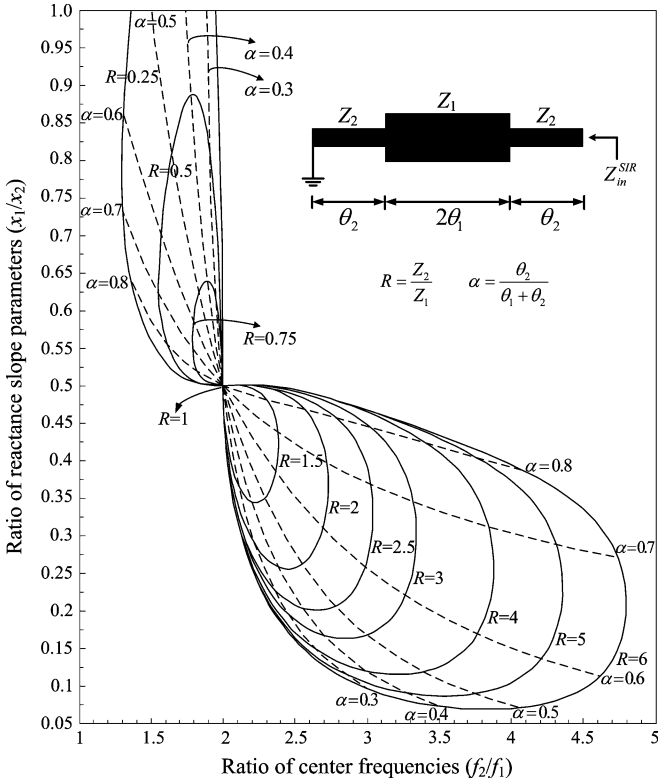

Fig. 6. Structural parameters of the SIR versus the ratios of center frequencies and reactance slope parameters.

C. Design of the External Coupling Circuit

The input and output ports are both achieved by a tapped feed line. The external quality factor Q_e of a singly loaded resonator is calculated as [23]

$$Q_e = \frac{g_0 g_1}{\Delta}. \tag{24}$$

The load impedance R_L seen at the tap point of the resonator is given as [23]

$$R_L = Q_e\left(\frac{\omega}{2}\frac{dB_T}{d\omega}\right)^{-1}|_{\omega=\omega_0} \tag{25}$$

where B_T is the total susceptance of the resonator seen at the tap point. Generally, the load impedance R_L may be different for the first and second passbands (i.e., $R_{L1} \neq R_{L2}$, where $R_{L1} = R_L|_{f=f_1}$ and $R_{L2} = R_L|_{f=f_2}$). We can choose R_L (e.g., $R_{L1} = R_{L2}$) and a tap position to obtain the filter response. A dual-frequency transformer [24] is used to match the 50-Ω input/output impedance to R_L at the tap position and accomplish the filter design.

IV. Design Examples

To demonstrate the validity of the proposed method, one fourth-order dual-band filter with f_2/f_1 smaller than 2 and one fourth-order and one sixth-order dual-band filter with f_2/f_1 larger than 2 were designed and implemented. All filters have a Chebyshev frequency response with a 0.1-dB ripple level. The circuits were fabricated on the Rogers RO4003 substrate with a dielectric constant of 3.6, a loss tangent of 0.0021, and

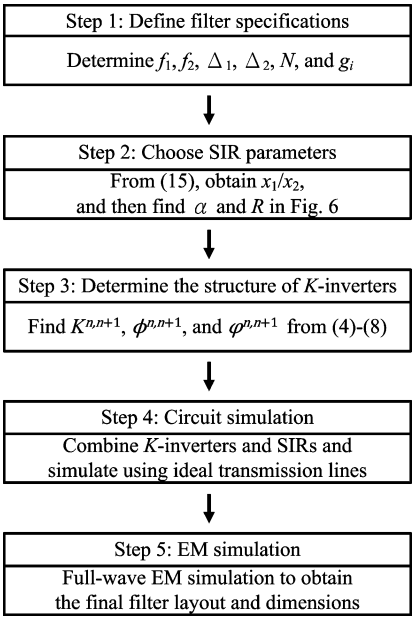

Fig. 7. Design flowchart of the proposed method.

a thickness of 0.508 mm. Each via-hole has a diameter of 0.3 mm. The circuit simulator AWR Microwave Office [25] and the full-wave EM simulation software Sonnet [26] were both used to perform the simulation. The measurements were carried out using an Agilent 8720ES network analyzer.

The design steps are outlined in Fig. 7 and are summarized as follows.

Step 1: Identify the dual-band filter specifications, including the center frequencies $(f_1,\ f_2)$, the fractional bandwidths $(\Delta_1,\ \Delta_2)$, the filter order (N), and the low-pass prototype elements $g_i,\ i = 0, 1, \ldots, N, N+1$.

Step 2: x_1/x_2 is calculated using (15). According to the design curves in Fig. 6, α and R are then selected. On the basis of α, R, and (2), θ_1 and θ_2 are obtained for $f = f_1$. We choose Z_2 first and then Z_1 is determined by R.

Step 3: From (4), the values of the K-inverters are available. According to the K values, $Z_d = Z_2$ and (5)–(7), we can get $b^{n,n+1}$ and $\phi^{n,n+1}$. We then choose $Z_K^{n,n+1}$ and substitute $Z_K^{n,n+1}$ and $b^{n,n+1}$ into (8) to obtain $\varphi^{n,n+1}$. Due to (9), the structure of the K-inverter is obtained from either the first or second passband.

Step 4: Combine the K-inverters and SIRs. Referring to Fig. 2(b) and (c), $\theta_{2,n} = \theta_2 + \phi^{n,n+1}$. The input and output ports are designed using the method in [24]. As a result, the response of the filter with ideal transmission lines (i.e., the inverters are also made of ideal transmission lines) can be simulated in the circuit simulator.

Step 5: Replace the ideal transmission line with the microstrip line and slightly fine tune the filter dimensions for optimal performance in the circuit simulator. Finally, the filter with the fine-tuned dimensions in the circuit simulator is simulated with a full-wave EM simulator to take the effects of via-holes, discontinuities, and junctions into account. The dual-band filter is then completed.

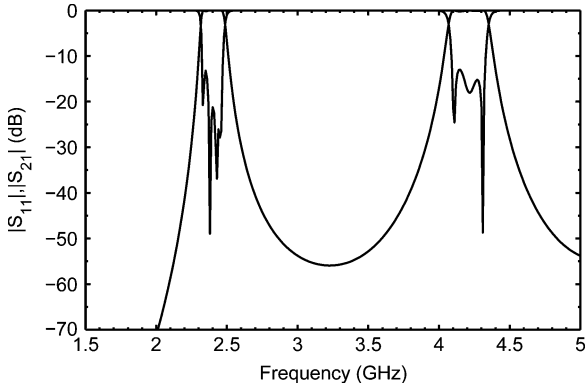

Fig. 8. Circuit simulation of the proposed filter I using ideal transmission lines and calculated results.

A. Fourth-Order Dual-Band Filter With $f_2/f_1 < 2$

The first example is a fourth-order dual-band filter with the center frequencies $f_1 = 2.4$ GHz and $f_2 = 4.2$ GHz (i.e., $f_2/f_1 < 2$). The fractional bandwidths of the two passbands are $\Delta_1 = \Delta_2 = 0.06$. For the fourth-order filter, the element values of the low-pass filter prototype are $g_0 = 1$, $g_1 = 1.10881$, $g_2 = 1.30618$, $g_3 = 1.77038$, $g_4 = 0.818081$, and $g_5 = 1.35538$. Applying (15), we have $f_2/f_1 = 1.75$ and $x_1/x_2 = 0.5714$. According to Fig. 6, the structural parameters of the SIR are found to be $R = 0.71$ and $\alpha = 0.66$. Substituting α and R into (2), $\theta_1 = 0.5834$ rad and $\theta_2 = 1.1325$ rad are obtained at f_1. In this example, $Z_2 = Z_d = 71\ \Omega$ are chosen so that $Z_1 = 100\ \Omega$ for $R = 0.71$.

The structure of the K-inverter can be obtained according to the first or second passband. Due to the structural symmetry, from (4), the K-inverters between resonators for the first and second passbands are obtained as $K_1^{12} = K_1^{34} = 5.7346$, $K_1^{23} = 4.5383$, $K_2^{12} = K_2^{34} = 9.9793$, and $K_2^{23} = 7.8976$. Here, we choose $Z_K^{1,2} = Z_K^{2,3} = Z_K^{3,4} = 86.35\ \Omega$ so that from (5)–(8) at f_1, $\varphi_1^{1,2} = \varphi_1^{3,4} = 0.06676$ rad and $\varphi_1^{2,3} = 0.05273$ rad, where subscript 1 denotes the first passband. The negative electrical lengths of the K-inverters are $\phi_1^{12} = \phi_1^{34} = -0.0806$ rad and $\phi_1^{23} = -0.0638$ rad. In this case, $\phi_2^{n,n+1}/\phi_1^{n,n+1} \approx f_2/f_1$. At f_1, the final electrical lengths of the SIRs are $\theta_{2,0} = \theta_{2,4} = \theta_2 = 1.1325$ rad, $\theta_{2,1} = \theta_{2,3} = \theta_2 + \phi_1^{12} = 1.0519$ rad, and $\theta_{2,2} = \theta_2 + \phi_1^{23} = 1.0687$ rad. The dual-frequency transformer is used to transform 50 to 197 Ω for the external coupling. From the calculated values, the circuit simulation using ideal transmission lines is shown in Fig. 8. Apparently, the response of the dual-band filter deviates slightly from the Chebyshev response, but it still performs well. The minor deviation is due to the fact that the K-inverters and the resonators are all designed only for the center frequencies and there are some simple approximations in the design procedure. Fig. 9 depicts the final physical layout and dimensions of the proposed dual-band filter. Here, we number these four resonators as 1–4 from top to bottom. Since W_2 is wide in this example, the influence of the T-junction effect on the K-inverter is obvious and should be taken into account.

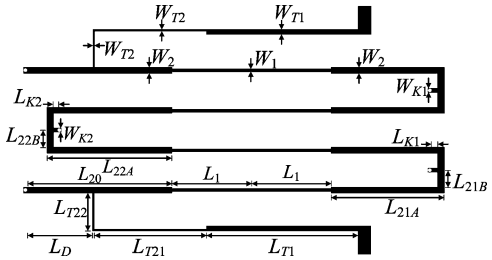

Fig. 9. Layout of the proposed fourth-order dual-band filter (filter I). Filter dimensions: $W_1 = 0.254$ mm, $W_2 = 0.5842$ mm, $W_{T1} = 0.4826$ mm, $W_{T2} = 0.127$ mm, $W_{K1} = W_{K2} = 0.381$ mm, $L_1 = 7.62$ mm, $L_{20} = 13.716$ mm, $L_{21A} = 10.668$ mm, $L_{21B} = 1.7145$ mm, $L_{22A} = 11.8364$ mm, $L_{22B} = 1.7145$ mm, $L_{T1} = 14.478$ mm, $L_{T21} = 10.668$ mm, $L_{T22} = 3.81$ mm, $L_D = 6.223$ mm, $L_{K1} = 0.635$ mm, and $L_{K2} = 0.4064$ mm.

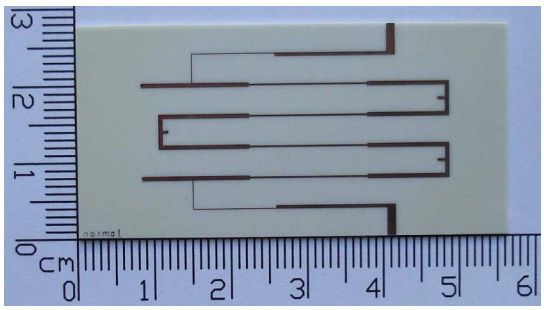

Fig. 10. Photograph of the fabricated fourth-order dual-band filter (filter I).

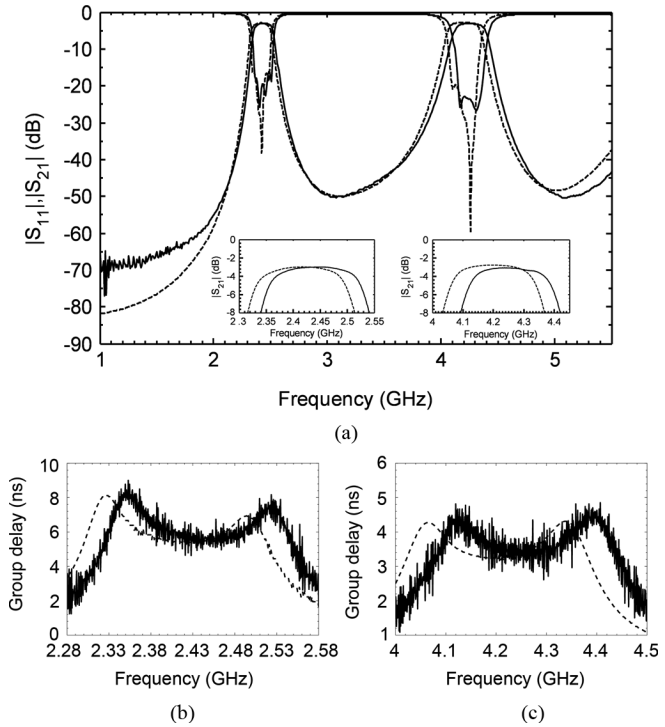

Fig. 11. Simulated (dashed line) and measured (solid line) results of the fourth-order dual-band filter (filter I). (a) Scattering parameters. (b) Group delay for the first passband. (c) Group delay for the second passband.

Fig. 10 presents the photograph of the fabricated dual-band filter I. The size of the filter is 39.9288 mm × 20.2946 mm, which is $0.5355\lambda_{g1} \times 0.2722\lambda_{g1}$, where λ_{g1} is the guided wavelength of the 50-Ω line on the substrate at the center frequency of the first passband. The simulated and measured results are illustrated in Fig. 11. For the first passband, the measured results show that the center frequency is 2.439 GHz, the minimum insertion loss is 2.992 dB, and the return loss is better than 16.05 dB. The passband group-delay variation is 2 ns. For the second passband, the center frequency is 4.257 GHz, the minimum insertion loss is 3.07 dB and the return loss is better than 22.97 dB. The passband group delay variation is 1 ns. The rejection level between the two passbands is better than 40 dB from 2.747 to 3.685 GHz. Compared to the simulated results, the measured center frequencies of the two passbands are slightly shifted toward higher frequencies. This is possibly due to the deviation of the dielectric constant. The insertion losses of the two passbands are slightly high in this case. This may be due to the narrow bandwidths and the high-impedance lines of the SIR and the dual-frequency transformer (i.e., narrow linewidth).

B. Fourth-Order Dual-Band Filter With $f_2/f_1 > 2$

The second example is a fourth-order dual-band filter with the center frequencies $f_1 = 1.8$ GHz and $f_2 = 5.2$ GHz (i.e., $f_2/f_1 > 2$). The fractional bandwidths of the two passbands are $\Delta_1 = 0.13$ and $\Delta_2 = 0.09$. The element values of the low-pass filter prototype are the same as those for filter I. Applying (15), $f_2/f_1 = 2.89$ and $x_1/x_2 = 0.24$ are obtained. From Fig. 6, the structural parameters of the SIR are obtained as $R = 2.41$ and $\alpha = 0.565$. Substituting R and α into (2), we have $\theta_1 = 0.5001$ rad and $\theta_2 = 0.6495$ rad at f_1. In this case, $Z_2 = Z_d = 86\ \Omega$ are chosen so that $Z_1 = 35.68\ \Omega$ for $R = 2.41$.

Following the same design procedure as described above, the K-inverters between resonators for the first and second passbands are calculated as $K_1^{12} = K_1^{34} = 11.3508$, $K_1^{23} = 8.983$, $K_2^{12} = K_2^{34} = 33.0447$, and $K_2^{23} = 26.1515$. Thus, at f_1, we have $Z_K^{1,2} = Z_K^{3,4} = 101\ \Omega$, $\varphi_1^{1,2} = \varphi_1^{3,4} = 0.1139$ rad, $Z_K^{2,3} = 69.6\ \Omega$, and $\varphi_1^{2,3} = 0.1298$ rad, where subscript 1 denotes the first passband. The negative electrical lengths of the K-inverters are $\phi_1^{12} = \phi_1^{34} = -0.1312$ rad and $\phi_1^{23} = -0.1041$ rad. At f_1, the final electrical lengths of the SIRs are $\theta_{2,0} = \theta_{2,4} = \theta_2 = 0.6495$ rad, $\theta_{2,1} = \theta_{2,3} = \theta_2 + \phi_1^{12} = 0.5183$ rad, and $\theta_{2,2} = \theta_2 + \phi_1^{23} = 0.5454$ rad. The external coupling is obtained using the dual-frequency transformer to transform 50 to 157 Ω. Fig. 12 shows the circuit simulation of the filter using ideal transmission lines based on the calculated results. In this case, the fractional bandwidths are larger than those of filter I. The ideal transmission line performance is worse than that of filter I, which might be due to the narrowband characteristics of the K-inverter. The final physical layout and dimensions of the filter are depicted in Fig. 13. Again, we number these four resonators as 1–4 from top to bottom. For resonators 1 and 4, there is a small capacitive gap between the T-junction and the SIR. The simulated result shows that this gap has little influence on the passband return losses.

Fig. 14 shows a photograph of the fabricated dual-band filter II. The size of the filter is 33.3248 mm × 20.5232 mm, i.e., $0.3352\lambda_{g1} \times 0.2064\lambda_{g1}$. Fig. 15 illustrates the simulated and measured responses. The measured results show that for the first passband, the center frequency is 1.7995 GHz. The

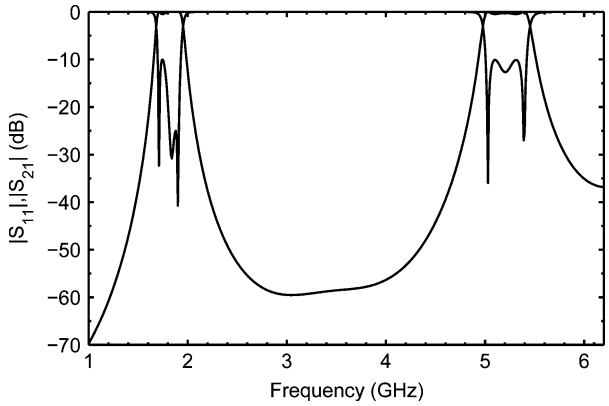

Fig. 12. Circuit simulation of the proposed filter II using ideal transmission lines and calculated results.

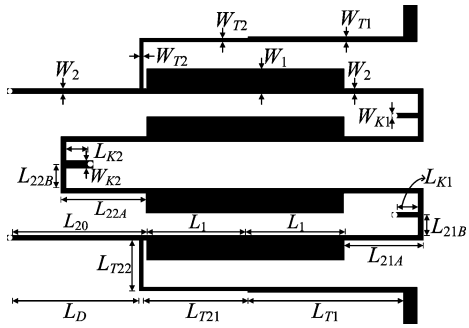

Fig. 13. Layout of the proposed fourth-order dual-band filter (filter II). Filter dimensions: $W_1 = 1.9558$ mm, $W_2 = 0.381$ mm, $W_{T1} = 0.4572$ mm, $W_{T2} = 0.3302$ mm, $W_{K1} = 0.254$ mm, $W_{K2} = 0.6096$ mm, $L_1 = 7.9248$ mm, $L_{20} = 10.8204$ mm, $L_{21A} = 6.35$ mm, $L_{21B} = 1.7018$ mm, $L_{22A} = 6.8834$ mm, $L_{22B} = 1.8796$ mm, $L_{T1} = 12.446$ mm, $L_{T21} = 8.3566$ mm, $L_{T22} = 4.0894$ mm, $L_D = 10.2616$ mm, $L_{K1} = 1.8288$ mm, and $L_{K2} = 1.9558$ mm.

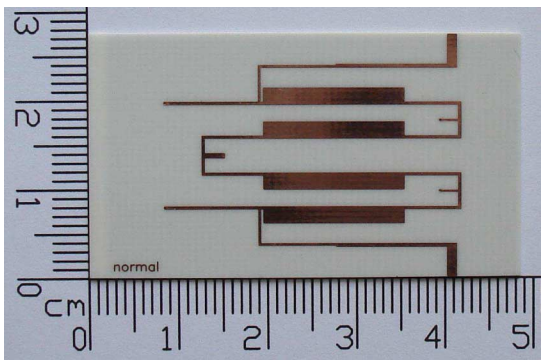

Fig. 14. Photograph of the fabricated fourth-order dual-band filter (filter II).

minimum insertion loss is 1.72 dB and the return loss is better than 18.9 dB. The measured 3-dB fractional bandwidth is 12.17% from 1.688 to 1.907 GHz. The passband group-delay variation is 1.5 ns. For the second passband, the center frequency is 5.205 GHz. The minimum insertion loss is 2.05 dB and the return loss is better than 20.41 dB. The measured 3-dB fractional bandwidth is 8.4% from 4.986 to 5.423 GHz. The passband group-delay variation is 0.6 ns. The rejection level between the two passbands is better than 40 dB from 2.203 to 3.978 GHz.

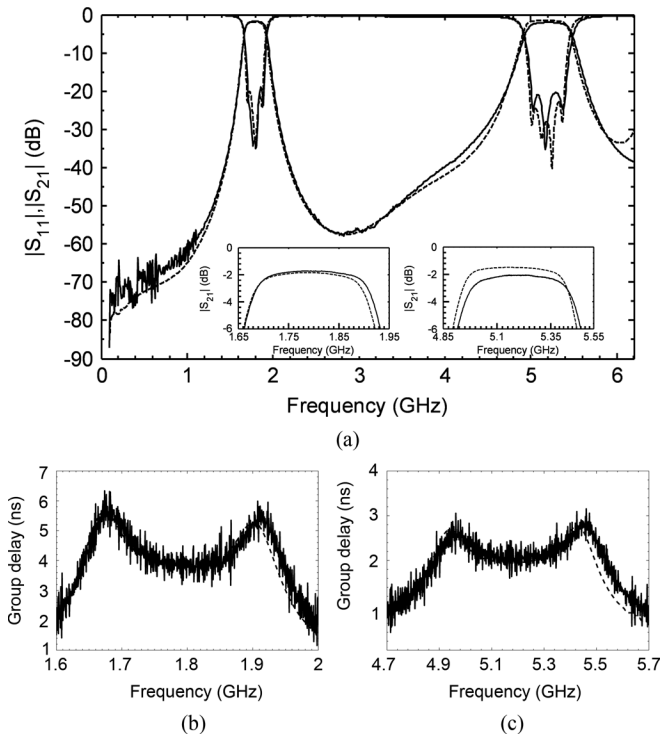

Fig. 15. Simulated (dashed line) and measured (solid line) results of the fourth-order dual-band filter (filter II). (a) Scattering parameters. (b) Group delay for the first passband. (c) Group delay for the second passband.

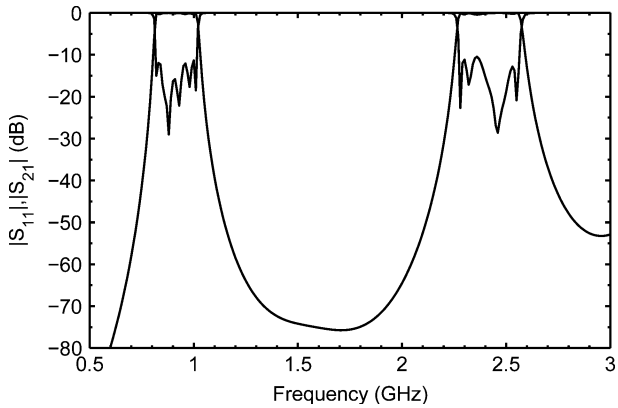

Fig. 16. Circuit simulation of the proposed filter III using ideal transmission lines and calculated results.

C. Sixth-Order Dual-Band Filter With $f_2/f_1 > 2$

To illustrate the facility of the proposed method to design a relatively high-order dual-band filter, a sixth-order dual-band filter is designed at the center frequencies $f_1 = 0.9$ GHz and $f_2 = 2.4$ GHz (i.e., $f_2/f_1 > 2$). The fractional bandwidths of the two passbands are $\Delta_1 = 0.21$ and $\Delta_2 = 0.12$. For the sixth-order filter, the element values of the low-pass filter prototype are $g_0 = 1$, $g_1 = 1.16814$, $g_2 = 1.40397$, $g_3 = 2.05623$, $g_4 = 1.51709$, $g_5 = 1.90291$, $g_6 = 0.861849$, and $g_7 = 1.35538$. First, from (15), $f_2/f_1 = 2.67$ and $x_1/x_2 = 0.214$ are obtained. Consequently, according to Fig. 6, the structural parameters of the SIR can be obtained as $R = 2.35$ and $\alpha = 0.48$. Substituting R and α into (2), we can get $\theta_1 = 0.6014$ rad and

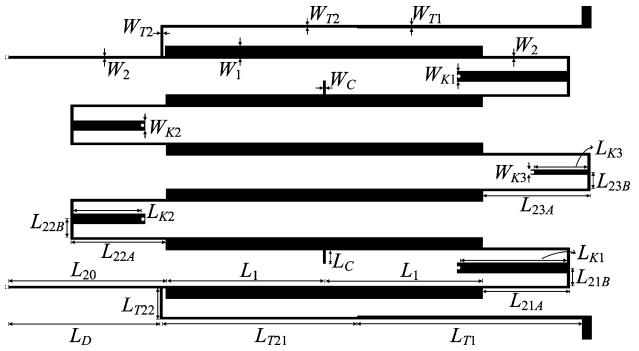

Fig. 17. Layout of the proposed sixth-order dual-band filter (filter III). Filter dimensions: $W_1 = 1.524$ mm, $W_2 = 0.254$ mm, $W_{T1} = 0.5334$ mm, $W_{T2} = 0.4064$ mm, $W_{K1} = 1.27$ mm, $W_{K2} = 1.143$ mm, $W_{K3} = 0.635$ mm, $W_C = 0.254$ mm, $L_1 = L_{20} = 18.923$ mm, $L_{21A} = 10.3886$ mm, $L_{21B} = 2.159$ mm, $L_{22A} = 11.43$ mm, $L_{22B} = 2.159$ mm, $L_{23A} = 12.7254$ mm, $L_{23B} = 1.9685$ mm, $L_{T1} = 26.8732$ mm, $L_{T21} = 23.0632$ mm, $L_{T22} = 3.81$ mm, $L_D = 18.2118$ mm, $L_{K1} = 12.954$ mm, $L_{K2} = 8.509$ mm, $L_{K3} = 6.5024$ mm, and $L_C = 1.6256$ mm.

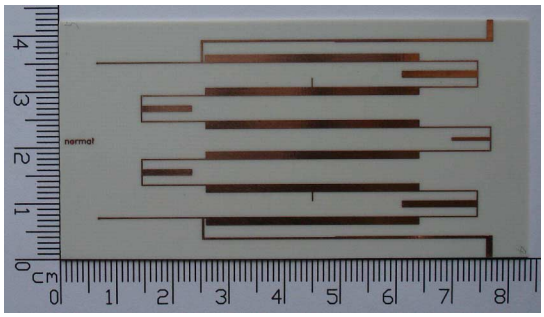

Fig. 18. Photograph of the fabricated sixth-order dual-band filter (filter III).

$\theta_2 = 0.5551$ rad at f_1. Here, $Z_2 = Z_d = 101\ \Omega$ are chosen so that $R = 2.35$ corresponds to $Z_1 = 43\ \Omega$.

Following the same design process, due to the structural symmetry, the K-inverters between resonators for the first and second passbands are found to be $K_1^{12} = K_1^{56} = 18.7559$, $K_1^{23} = K_1^{45} = 14.1367$, $K_1^{34} = 13.5995$, $K_2^{12} = K_2^{56} = 49.6137$, $K_2^{23} = K_2^{45} = 37.395$, and $K_2^{34} = 35.9738$. Thereby, from (5) to (8) at f_1, we have $Z_K^{1,2} = Z_K^{5,6} = 45.9\ \Omega$, $\varphi_1^{1,2} = \varphi_1^{5,6} = 0.4004$ rad, $Z_K^{2,3} = Z_K^{4,5} = 49\ \Omega$, $\varphi_1^{2,3} = \varphi_1^{4,5} = 0.2862$ rad, $Z_K^{3,4} = 68.3\ \Omega$, and $\varphi_1^{3,4} = 0.2001$ rad, where subscript 1 denotes the first passband. The negative electrical lengths of the K-inverters are $\phi_1^{12} = \phi_1^{56} = -0.1836$ rad, $\phi_1^{23} = \phi_1^{45} = -0.1391$ rad, and $\phi_1^{34} = -0.1339$ rad. At f_1, the final electrical lengths of the SIRs are $\theta_{2,0} = \theta_{2,6} = \theta_2 = 0.5551$ rad, $\theta_{2,1} = \theta_{2,5} = \theta_2 + \phi_1^{12} = 0.3715$ rad, $\theta_{2,2} = \theta_{2,4} = \theta_2 + \phi_1^{23} = 0.416$ rad, and $\theta_{2,3} = \theta_2 + \phi_1^{34} = 0.4212$ rad. The dual-frequency transformer is adopted to transform 50 to 128 Ω for the external coupling. According to the calculated values, the response of the filter with ideal transmission lines is shown in Fig. 16. Compared to the Chebyshev response, the ideal transmission line performance deviates slightly due to the simple approximations in the design procedure and narrowband characteristics of the K-inverter. The final physical layout and dimensions of the dual-band filter are given in Fig. 17, where we number these six resonators as 1–6 from top to bottom. Note that, in this example, due to the larger bandwidths compared to the previous two examples, two open stubs are added on the middle

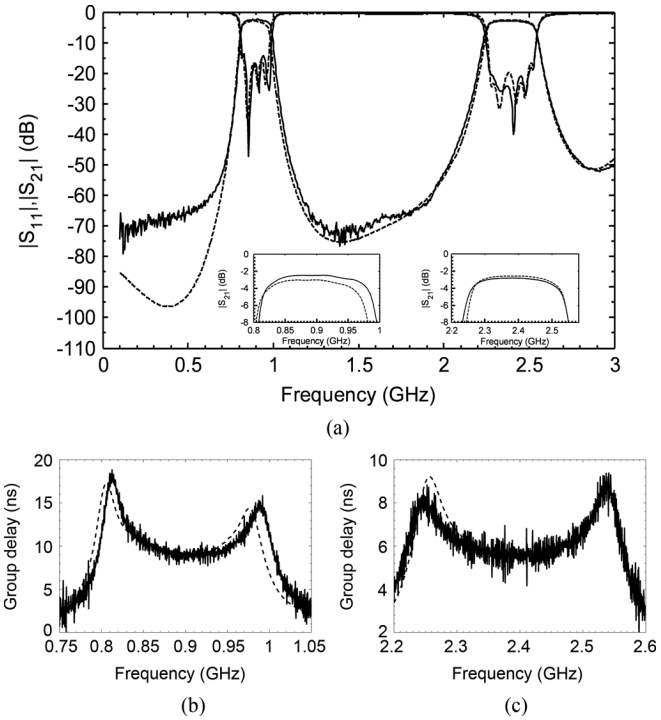

Fig. 19. Simulated (dashed line) and measured (solid line) results of the sixth-order dual-band filter (filter III). (a) Scattering parameters. (b) Group delay for the first passband. (c) Group delay for the second passband.

of resonators 2 and 5 so as to compensate for the electrical lengths of the first passband.

Fig. 18 shows a photograph of the fabricated dual-band filter III. The size of the filter is 69.7992 mm $\times$ 35.433 mm, which is $0.3511\lambda_{g1} \times 0.1782\lambda_{g1}$. The simulated and measured results are presented in Fig. 19. For the first passband, the measured results show that the center frequency is 0.90015 GHz, the minimum insertion loss is 2.471 dB, and the return loss is better than 14.07 dB. The passband group-delay variation is 7 ns. For the second passband, the center frequency is 2.3925 GHz, the minimum insertion loss is 2.816 dB, and the return loss is better than 18.25 dB. The passband group delay variation is 3 ns. The rejection level between the two passbands is better than 40 dB from 1.068 to 2.103 GHz.

V. Conclusion

A simple and time-saving method to design dual-band filters has been presented in this paper. Since the ratio of the first and second resonances and the ratio of the first and second fractional bandwidths are easily controlled, the short-circuit terminated half-wavelength SIR is used to realize a filter with dual passbands. With the aid of the design graph for SIRs, the structure of the SIR is easily obtained according to the filter specifications. Furthermore, the available filter specifications can be quickly examined. The coupling between adjacent SIRs is easily achieved by a short-circuited stub, which is characterized as a K-inverter. Accordingly, the narrow gap between resonators is avoided so that the filter specifications are less constrained. The equations between the K-inverter and the filter specifications are analytically derived. Due to the analytical design equations in the proposed method, the filter can be first simulated using the conventional circuit simulator and the time-consuming EM

simulation is adopted in the final step. The proposed method especially follows the regular design process and is very appropriate to apply to the relatively high-order dual-band filter design. Two fourth-order and one sixth-order dual-band filters were constructed to demonstrate the proposed method. Good agreement between measurements and simulations is observed.

REFERENCES

[1] H. Miyake, S. Kitazawa, T. Ishizaki, T. Yamada, and Y. Nagatomi, "A miniaturized monolithic dual band filter using ceramic lamination technique for dual mode portable telephones," in *IEEE MTT-S Int. Microw. Symp. Dig.*, Jun. 1997, vol. 2, pp. 789–792.

[2] L. C. Tsai and C. W. Hsue, "Dual-band bandpass filters using equal-length coupled-serial-shunted lines and Z-transform technique," *IEEE Trans. Microw. Theory Tech.*, vol. 52, no. 4, pp. 1111–1117, Apr. 2004.

[3] C. Quendo, E. Rius, and C. Person, "An original topology of dual-band filter with transmission zeros," in *IEEE MTT-S Int. Microw. Symp. Dig.*, Jun. 2003, vol. 2, pp. 1093–1096.

[4] C. M. Tsai, H. M. Lee, and C. C. Tsai, "Planar filter design with fully controllable second passband," *IEEE Trans. Microw. Theory Tech.*, vol. 53, no. 11, pp. 3429–3439, Nov. 2005.

[5] H. M. Lee and C. M. Tsai, "Dual-band filter design with flexible passband frequency and bandwidth selections," *IEEE Trans. Microw. Theory Tech.*, vol. 55, no. 5, pp. 1002–1009, May 2007.

[6] C. Y. Chen and C. Y. Hsu, "A simple and effective method for microstrip dual-band filters design," *IEEE Microw. Wireless Compon. Lett.*, vol. 16, no. 5, pp. 246–248, May 2006.

[7] J. X. Chen, T. Y. Yum, J. L. Li, and Q. Xue, "Dual-mode dual-band bandpass filter using stacked-loop structure," *IEEE Microw. Wireless Compon. Lett.*, vol. 16, no. 9, pp. 502–504, Sep. 2006.

[8] M. H. Weng, C. Y. Huang, H. W. Wu, K. Shu, and Y. K. Su, "Compact dual-band bandpass filter with enhanced feed coupling structures," *Microw. Opt. Technol. Lett.*, vol. 49, no. 1, pp. 171–173, Jan. 2007.

[9] X. Y. Zhang, J. Shi, J. X. Chen, and Q. Xue, "Dual-band bandpass filter design using a novel feed scheme," *IEEE Microw. Wireless Compon. Lett.*, vol. 19, no. 6, pp. 350–352, Jun. 2009.

[10] X. Y. Zhang, J. X. Chen, Q. Xue, and S. M. Li, "Dual-band bandpass filters using stub-loaded resonators," *IEEE Microw. Wireless Compon. Lett.*, vol. 17, no. 8, pp. 583–585, Aug. 2007.

[11] P. Mondal and M. K. Mandal, "Design of dual-band bandpass filters using stub-loaded open-loop resonators," *IEEE Trans. Microw. Theory Tech.*, vol. 56, no. 1, pp. 150–155, Jan. 2008.

[12] M. Zhou, X. Tang, and F. Xiao, "Compact dual band bandpass filter using novel E-type resonators with controllable bandwidths," *IEEE Microw. Wireless Compon. Lett.*, vol. 18, no. 12, pp. 779–781, Dec. 2008.

[13] S. F. Chang, Y. H. Jeng, and J. L. Chen, "Dual-band step-impedance bandpass filter for multimode wireless LANs," *Electron. Lett.*, vol. 40, no. 1, pp. 38–39, Jan. 2004.

[14] H. M. Lee, C. R. Chen, C. C. Tsai, and C. M. Tsai, "Dual-band coupling and feed structure for microstrip filter design," in *IEEE MTT-S Int. Microw. Symp. Dig.*, Jun. 2004, vol. 3, pp. 1971–1974.

[15] J. T. Kuo, T. H. Yeh, and C. C. Yeh, "Design of microstrip bandpass filters with a dual-passband response," *IEEE Trans. Microw. Theory Tech.*, vol. 53, no. 4, pp. 1331–1337, Apr. 2005.

[16] S. Sun and L. Zhu, "Compact dual-band microstrip bandpass filter without external feeds," *IEEE Microw. Wireless Compon. Lett.*, vol. 15, no. 10, pp. 644–646, Oct. 2005.

[17] C. F. Chen, T. Y. Huang, and R. B. Wu, "Design of dual- and triple-passband filters using alternately cascaded multiband resonators," *IEEE Trans. Microw. Theory Tech.*, vol. 54, no. 9, pp. 3550–3558, Sep. 2006.

[18] Y. P. Zhang and M. Sun, "Dual-band microstrip bandpass filter using stepped-impedance resonators with new coupling schemes," *IEEE Trans. Microw. Theory Tech.*, vol. 54, no. 10, pp. 3779–3785, Oct. 2006.

[19] M. H. Weng, H. W. Wu, and Y. K. Su, "Compact and low loss dual-band bandpass filter using pseudo-interdigital stepped impedance resonators for WLANs," *IEEE Microw. Wireless Compon. Lett.*, vol. 17, no. 3, pp. 187–189, Mar. 2007.

[20] C. H. Tseng and H. Y. Shao, "A new dual-band microstrip bandpass filter using net-type resonators," *IEEE Microw. Wireless Compon. Lett.*, vol. 20, no. 4, pp. 196–198, Apr. 2010.

[21] F. C. Chen and Q. X. Chu, "Novel multistub loaded resonator and its application to high-order dual-band filters," *IEEE Trans. Microw. Theory Tech.*, vol. 58, no. 6, pp. 1551–1556, Jun. 2010.

[22] M. Makimoto and S. Yamashita, *Microwave Resonators and Filters for Wireless Communication: Theory, Design and Application*. Berlin, Germany: Springer-Verlag, 2001.

[23] G. L. Matthaei, L. Young, and E. M. T. Jones, *Microwave Filters, Impedance-Matching Networks and Coupling Structures*. Norwood, MA: Artech House, 1980.

[24] C. Monzon, "A small dual-frequency transformer in two sections," *IEEE Trans. Microw. Theory Tech.*, vol. 51, no. 4, pp. 1157–1161, Apr. 2003.

[25] *"Reference Guide Microwave Office,"* AWR, El Segundo, CA, 2003.

[26] *"Em User's Manual,"* Sonnet Softw., Liverpool, NY, 2004.

Wei-Shin Chang was born in Taipei, Taiwan, on September 15, 1986. She received the B.S. degree in physics from National Taiwan Normal University, Taipei, Taiwan, in 2009, and is currently working toward the Ph.D. degree in communication engineering at National Chiao-Tung University, Hsinchu, Taiwan.

Her research interests include the analysis and design of periodic structures and microwave circuits.

Chi-Yang Chang (M'95) was born in Taipei, Taiwan, on December 20, 1954. He received the B.S. degree in physics and M.S. degree in electrical engineering from National Taiwan University, Taipei, Taiwan, in 1977 and 1982, respectively, and the Ph.D. degree in electrical engineering from The University of Texas at Austin, in 1990.

From 1990 to 1995, he was an Associate Researcher with the Chung-Shan Institute of Science and Technology (CSIST), where he was in charge of development of uniplanar circuits, ultra-broadband circuits, and millimeter-wave planar circuits. In 1995, he joined the faculty of the Department of Communication Engineering (renamed the Department of Electrical Engineering in 2009), National Chiao-Tung University, Hsinchu, Taiwan, as an Associate Professor, and became a Professor in 2002. His research interests include microwave and millimeter-wave passive and active circuit design, planar miniaturized filter design, and monolithic-microwave integrated-circuit (MMIC) design.